ACS OMEGA

Open Access



http://pubs.acs.org/journal/acsodf

Article

# Sulfuric Acid Baking and Fe(III)-$Cl^-$-$H_2SO_4$ Leaching Behavior of Ni- and Cu-Containing Sulfide and Silicate Rich Suhanko Concentrate

Pingchao Ke,* Marja Rinne, Taina Kalliomäki, Zulin Wang, Pyry-Mikko Hannula, Benjamin P. Wilson, and Mari Lundström*

Cite This: *ACS Omega* 2024, 9, 26121−26132

Read Online

ACCESS | Metrics & More | Article Recommendations | Supporting Information

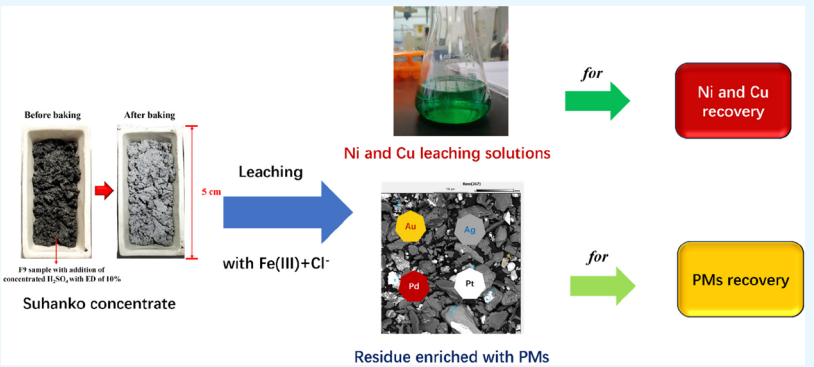


**ABSTRACT:** Ni- and Cu-rich concentrate from a new site in Suhanko, Finland, was investigated. Mineral phases identified included talc, chalcopyrite, kaolinite, and pyrrhotite with 3.2% Cu and 1.5% Ni, and the latter is associated with pyrrhotite. In addition, the concentrate contained the precious elements Pd (14.9 g/t), Ag (17.1 g/t), Pt (2.1 g/t), and Au (1.1 g/t). This concentrate was baked and leached using a Fe(III)-$Cl^-$-$H_2SO_4$ system. The results showed that the leaching efficiencies of Ni, Cu, and Si from raw concentrate were 60%, 40%, and 5%; however, those from baked concentrate were 96%, 60%, and below 0.1%, indicating that the baking process enhanced Ni and Cu extraction while simultaneously inhibiting the dissolution of Si, which was due to the baking process liberating the associated Ni and Cu by the oxidation of chalcopyrite and pyrrhotite and converting the acid-soluble silicate into an insoluble form. Sulfuric acid leaching solution with Fe(III) as oxidant and $Cl^-$ as lixiviant was shown to be effective at leaching Ni (97%), Cu (62%), and Ag (89%), while simultaneously enriching the PMs Pd, Pt, and Au in the residue.

## 1. INTRODUCTION

Nickel and copper are vital metals for society that are playing an increasingly important role in the drive toward a more sustainable global economy.[1,2] Nevertheless, due to the rapid development and wide use of Li-ion batteries (LIBs) in many aspects of everyday life, nickel supply shortages have led to sharp increases in Ni prices over the past decade.[3,4] Although the recycling of spent LIBs offers an accessible Ni and Cu secondary raw material source, nevertheless, only a part of spent LIBs is being recycled, and the amounts of recycled materials cannot fulfill the global battery metals demand alone. Consequently, there is an increased need to discover new sources for Ni and Cu that can be sustainably processed such that the maximum elemental and monetary value of these primary reserves is realized.[5]

Among the numerous Ni and Cu minerals, Chalcopyrite ($CuFeS_2$) and Ni-sulfide minerals are widely recognized as the most important Cu- and Ni-bearing ores.[6] In addition to the dominating elements, chalcopyrite and Ni-sulfide minerals are typically associated with platinum group metals (PGMs) minerals.[7,8] Moreover, the content of precious elements (Au, Ag, Pd, and Pt) in chalcopyrite and pyrrhotite are generally only determined once the flotation−separation step of Ni and Cu concentrates from Ni-Cu-PGM ores is completed.[9,10]

Various methods for metals extraction from chalcopyrite have been utilized. These include iron cementation via natural weathering processes (ca. 1100 A.D.);[11] ammonia pressure leaching;[12] ferric chloride leaching followed by either electro-dissolution-deposition (Cymet Process[13]); or solvent extraction and electrowinning (MINTEK process[14]). Other $H_2SO_4$-based pressure leaching methods for Ni and Cu recovery have also been developed, and the effect of parameters on the leaching mechanism has been extensively studied.[15] Addition-

Received: February 18, 2024
Revised: May 24, 2024
Accepted: May 28, 2024
Published: June 7, 2024

ally, the use of chlorides within leaching processes has increased interest.[16−20]

As with chalcopyrite, hydrometallurgical processes for Ni extraction from the primary Ni sulfide mineral pentlandite have been extensively researched and are dominated by ammonia, sulfate, and chloride leaching processes.[21−24] Of these, the faster kinetics relative to the sulfate for Ni and Cu recovery provided by chloride-based methods are preferred due to general association of pentlandite with both chalcopyrite and pyrrhotite.[25] Other processes used for Ni and Cu extraction from a wide range of Cu-Ni-bearing minerals include oxidant including $Cu^{2+}$, $Fe^{3+}$, or $O_2$ assisted halide recovery (Intec)[26] and high temperature oxygen pressure leaching (Platsol).[27,28]

Raw material including PGMs bearing ores, PGM concentrate, and PGM bearing matte are generally treated with a pressure leaching process using halides, $H_2SO_4$, or cyanide lixiviant with $O_2$, $Cl_2$, or $HNO_3$ oxidant followed by a recovery process including precipitation, metal cementation, carbon adsorption, ion exchange (IX), solvent extraction (SX), electrowinning (EW), or SX-EW.[29−31]

To improve the leaching efficiency from refractory ores, especially high silicate bearing ores, many pretreatment processes such as roasting,[32,33] bio-oxidation,[34,35] and baking[36] have been used to either activate or passivate the targeted phases. Among these processes, baking with sulfuric acid is the most common process used to pretreat high silicate bearing ores like calamine and manganite, as it allows the conversion of acid-soluble silicate into an insoluble form at relatively low temperatures (25−300 °C), controlling the leaching of Si.[37] This pretreatment step prevents the formation of $H_2SiO_3$, which can result in gel-like solids that seriously impact the leach residue filtration and metal recovery.[38] During baking, silicate reacts with sulfuric acid to form sulfate and acid-insoluble $SiO_2$, while any sulfidic constituents present in pyrrhotite and chalcopyrite can be oxidized into sulfate and $SO_2$. The main reaction that occurs in baking is described as eq 1, with side reactions of eqs 2 and 3.

$$MSiO_{3(s)} + H_2SO_4(\text{concentrated}) \rightarrow MSO_{4(s)} + SiO_{2(s)} + H_2O_{(g/l)} \quad (1)$$

$$Fe_{1-x}S_{(s)} + (2-x)O_{2(g)} \rightarrow (1-x)FeSO_{4(s)} + xSO_2 \quad (2)$$

$$2CuFeS_{2(s)} + 5O_{2(g)} \rightarrow Cu_2S_{(s)} + 2FeSO_{4(s)} + SO_{2(g)} \quad (3)$$

where M = Ca, Mg, Al, Ni, Cu, Fe, etc.

A new type of Ni- and Cu-containing sulfide and silicate rich concentrate from the Ahmavaara deposit in Suhanko, Finland, was studied. Originally, 50.8 tonnes of drill core was selected from the mineralized intervals of a total of 142 diamond drill holes. Then, sample material was transported for pilot plant flotation test work and to generate enough concentrate for further hydrometallurgical testing. Initial analysis of the concentrate identified talc ($Mg_3SiO_{10}(OH)_2$), chalcopyrite ($CuFeS_2$), and pyrrhotite ($Fe_{1-x}S$) as the main mineral phases present, along with relatively high levels Ni, Cu, Si, and precious metals (PMs) that included Pd, Pt, Au, and Ag. The current recovery process indicates that the valuable metals were leached with an extremely high concentration of acid and assistance of oxidant, and then, PMs were recovered by electrowinning. However, a significant amount of Si dissolved into the solution, seriously affecting the filtering and electrowinning processes.

Therefore, in our research with processing a Ni- and Cu-containing sulfide and silicate rich concentrate Ni, a comparison of sulfuric acid baking and Fe(III)-Cl-$H_2SO_4$ leaching processes was investigated for confirming the significant role of the baking process and Fe(III) and $Cl^-$ on the inhibition of Si leaching and promotion of Ni and Cu extraction as well as enrichment of PMs.

## 2. EXPERIMENTAL SECTION

**2.1. Raw Materials.** A new ore fraction (approximately 50 t) was extracted from the Ahmavaara deposit in Suhanko and subjected to primary flotation and two-stage cleaning to produce a concentrate. A sample of the concentrate was dried at 60 °C for 31 h before being ground until the material could be passed through a 4 mm mesh sieve. After grinding, the concentrate was homogeneously divided into ten fractions (F1−F10, on average 2680 g) by a rotating sample divider (Retsch PT600XL, Germany).

From these fractions, fraction F9 was selected for further investigation. Samples were characterized with X-ray diffraction (XRD, PANalytical X'Pert Pro Powder, The Netherlands) to identify the mineral phases. In addition, scanning electron microscopy with energy dispersive spectroscopy (SEM: LEO 1450, Carl Zeiss Microscopy GmbH, Germany; EDS: Link Inca X-sight 7366, UK) was also used to determine the morphology and elemental distribution. Chemical composition of samples was analyzed by Inductively Coupled Plasma-Optical Emission Spectrometry (ICP-OES, PerkinElmer Optima 7100DV; iCAP 6500, Thermo Fisher Scientific), ICP-MS (iCAP Qc, Thermo Fisher Scientific), and FAAS (Varian AA240) techniques following an acid digestion step. Precious metals in the sample were determined via fire assay.

**2.2. Baking.** According to eq 1, the possible reactions in the baking for the concentrate are shown in Tabel 1 and their standard Gibbs free energies at the preset temperature of 250 °C were determined.

**Table 1. Standard Gibbs Free Energy for the Possible Baking Reaction at 250 °C**

| Reaction | $\Delta G^{\theta}$(523 K) (kJ/mol) |
|---|---|
| $CaSiO_3 + H_2SO_4(\text{concentrated}) \rightarrow CaSO_{4(s)} + SiO_{2(s)} + H_2O_{(g/l)}$ | −174.09 |
| $MgSiO_3 + H_2SO_4(\text{concentrated}) \rightarrow MgSO_{4(s)} + SiO_{2(s)} + H_2O_{(g/l)}$ | −82.24 |
| $Al_2SiO_5 + 3H_2SO_4(\text{concentrated}) \rightarrow Al_2(SO_4)_3 + SiO_{2(s)} + 3H_2O_{(g/l)}$ | −136.42 |
| $FeSiO_3 + H_2SO_4(\text{concentrated}) \rightarrow FeSO_{4(s)} + SiO_{2(s)} + H_2O_{(g/l)}$ | −105.88 |

Through the analysis of the raw concentrate, Ni, Cu, and Fe exist as the sulfide phase, and Ca, Mg, and Al as silicates, and the Fe-Si phase could not be excluded due to its high content. As can be seen from Table 1, the theoretical molar ratio of concentrated $H_2SO_4$ was equal to that of possible phases $CaSiO_3$, $MgSiO_3$, and $FeSiO_3$, but the molar ratio was 1:3 for $Al_2SiO_5$ to concentrated $H_2SO_4$. Due to a relatively low content of Al compared to Ca, Mg, and Fe, the theoretical dosage of $H_2SO_4$ was very close to the molar amount of Si.

The theoretical dosage (TD) required for a molar ratio of 1:1 $H_2SO_4$:$SiO_3^{2-}$ to ensure efficient baking is 48 g of


https://doi.org/10.1021/acsomega.4c01560
ACS Omega 2024, 9, 26121−26132

concentrated $H_2SO_4$ (98%) per 100 g of sample. An excess dosage (ED) of 0−20 g of $H_2SO_4$/100 g of sample was used to ensure the full transformation of $SiO_2$ to the acid insoluble form. The total dosage of concentrated $H_2SO_4$ added was calculated with eq. 4:

$$\text{Total dosage of concentrated } H_2SO_4 = \text{TD} + \text{ED} \quad (4)$$

where TD = 48% of the total mass of sample; ED = 0−20% of the total mass of sample.

For the sulfuric acid baking step, 5 g of the concentrate was placed into a ceramic crucible (5 cm × 1.5 cm × 0.5 cm), and then concentrated $H_2SO_4$ (theoretical dosage of 48% + excess dosage of 0−20%) was slowly added to the crucible and mixed with a glass rod. The crucible was then heated at 200−300 °C for 3−5 h in a horizontal tube furnace (GSL-1700X, Shjingmi, Ltd., China) with a gas cleaning system to capture any $SO_2$ and $SO_3$ released during the process. After heating, the crucible was removed from the furnace and allowed to cool in ambient air. The newly baked sample (named RF9) was then characterized with XRD and SEM to determine any phase and morphological changes. Sample chemical analysis was conducted by total leaching followed by ICP-OES and ICP-MS analyses.

**2.3. Leaching.** To leach Ni and Cu and enrich PMs, leaching experiments for both the untreated (F9) and baked concentrates were carried out with $H_2SO_4$ solution in a 1 L glass reactor with 400 rpm stirring. Sulfuric acid solutions with different concentrations (30, 50, 80, 100 g/L) were used for leaching. Analytical grade chemicals, $Fe_2(SO_4)_3{\cdot}9H_2O$ and NaCl (≥98%, technical, VWR), were used as a supportive oxidant and lixiviant, respectively. The parameters used in the leaching experiments are outlined in Table 2.

**Table 2. Parameters of the Leaching Tests Series**

| No. | Raw materials | Reaction time (h) | S/L (g/L) | $H_2SO_4$ (g/L) | Fe(III) (g/L) | $Cl^-$ (g/L) | T (°C) |
|---|---|---|---|---|---|---|---|
| T1 | F9 | 3 | 50 | 50 | 5.0 | 0 | 90 |
| T2 | RF9 | 3 | 50 | 50 | 5.0 | 0 | 90 |
| T3 | F9 | 3 | 50 | 50 | 5.0 | 20 | 90 |
| T4 | RF9 | 3 | 50 | 50 | 5.0 | 20 | 90 |
| T5 | RF9 | 5 | 50 | 50 | 10 | 0 | 90 |
| T6 | RF9 | 5 | 50 | 50 | 10 | 20 | 90 |
| T7 | RF9 | 3 | 50 | 50 | 0 | 20 | 90 |
| T8 | RF9 | 3 | 50 | 50 | 2.5 | 20 | 90 |
| T9 | RF9 | 3 | 50 | 50 | 5 | 10 | 90 |
| T10 | RF9 | 3 | 50 | 50 | 5 | 2.5 | 90 |
| T11 | RF9 | 3 | 50 | 50 | 5 | 30 | 90 |
| T12 | RF9 | 3 | 50 | 50 | 5 | 5 | 90 |
| T13 | RF9 | 3 | 50 | 100 | 5 | 20 | 90 |
| T14 | RF9 | 3 | 50 | 30 | 5 | 20 | 90 |
| T15 | RF9 | 3 | 50 | 80 | 5 | 20 | 90 |
| T16 | RF9 | 3 | 50 | 50 | 5 | 20 | 30 |
| T17 | RF9 | 3 | 50 | 50 | 5 | 20 | 50 |
| T18 | RF9 | 3 | 50 | 50 | 5 | 20 | 70 |

During the experiments, the leaching slurry was periodically sampled. The slurry samples were filtered through a syringe filter, and then the filtrate was analyzed by ICP-OES for Ni, Fe, Cu, Mg, Al, and Si and by ICP-MS for Pd, Pt, Au, and Ag. The residue was characterized by SEM-EDS and subjected to acid digestion followed by ICP-OES, ICP-MS, and FAAS elemental analyses.

The redox potential and pH of the final pregnant leaching solution (PLS) was measured with a redox electrode and pH meter.

## 3. RESULTS AND DISCUSSION

**3.1. Characterization of Raw Material.** The main mineral phases present in the concentrate were talc ($Mg_3Si_4O_{10}(OH)_2$), chalcopyrite ($CuFeS_2$), pyrrhotite ($Fe_{1-x}S$), and kaolinite ($Al_2Si_2O_5(OH)_4$), confirmed by XRD, Figure 1. The

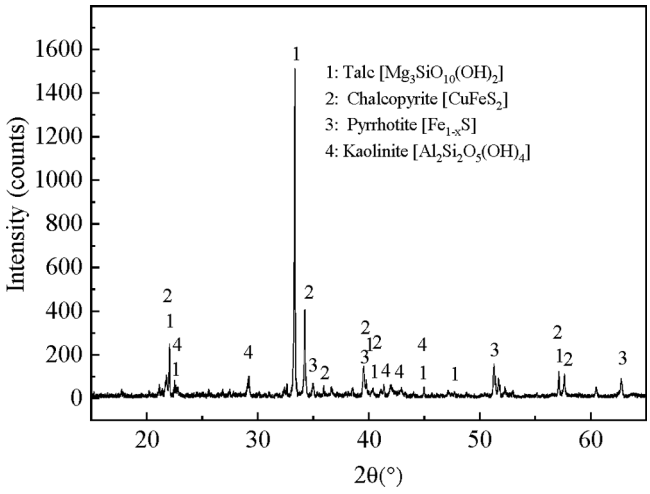


**Figure 1.** XRD pattern of the raw concentrate sample.

percentage for each phase was calculated by using the software *HighScrore*, and 78.7% pyrrhotite, 3.5% chalcopyrite, 11.8% kaolinite, and 6.0% talc were determined through the calculation.

The composition of the concentrate was determined by chemical analysis. The contents of Ni and Cu in the concentrate were 1.5% and 3.2%, respectively, and PMs including Pd, Ag, Pt, and Au and other elements (>1%) including Fe, S, Si, Mg, Al, and Ca are summarized in Table 3.

**Table 3. Contents of the Base Elements (BEs) and PMs of the Concentrate, Analyzed by ICP-OES*, ICP-MS***, or FAAS*****

| BEs | Fe* | S* | Si* | Mg* | Cu* | Al* | Ni* | Ca* |
|---|---|---|---|---|---|---|---|---|
| wt % | 24.1 | 15.3 | 14.0 | 7.38 | 3.23 | 1.98 | 1.47 | 1.14 |
| **PMs** | **Pd*** ** | **Ag[a]** | **Pt*** ** | **Au*** ** | | | | |
| g/t | 14.93 | 17.12 | 2.10 | 1.07 | | | | |

[a]The data of Ag content was provided by Suhanko Arctic Platinum and was determined with the NiS fire assay.

As can be seen from Figure 2a, there are two types of particles in the concentrate with random morphology and particle sizes between 10 and 100 μm. Seven-point analyses (EDS) were conducted, Figure 2b. The content of elements including O, Mg, Al, Si, S, Fe, Cu, and Ni in every point was detected as summarized in Table S1 (Supporting Information). Thereby the mineral phases were suggested to contain chalcopyrite and pyrrhotite, whereas particles presenting low contrast mainly contain talc and kaolinite.

Figure 3 shows the EDS mapping analyses including elemental distribution and quantitative energy spectra analysis (Figure S1 in the Supporting Information). The distributions



https://doi.org/10.1021/acsomega.4c01560
ACS Omega 2024, 9, 26121−26132

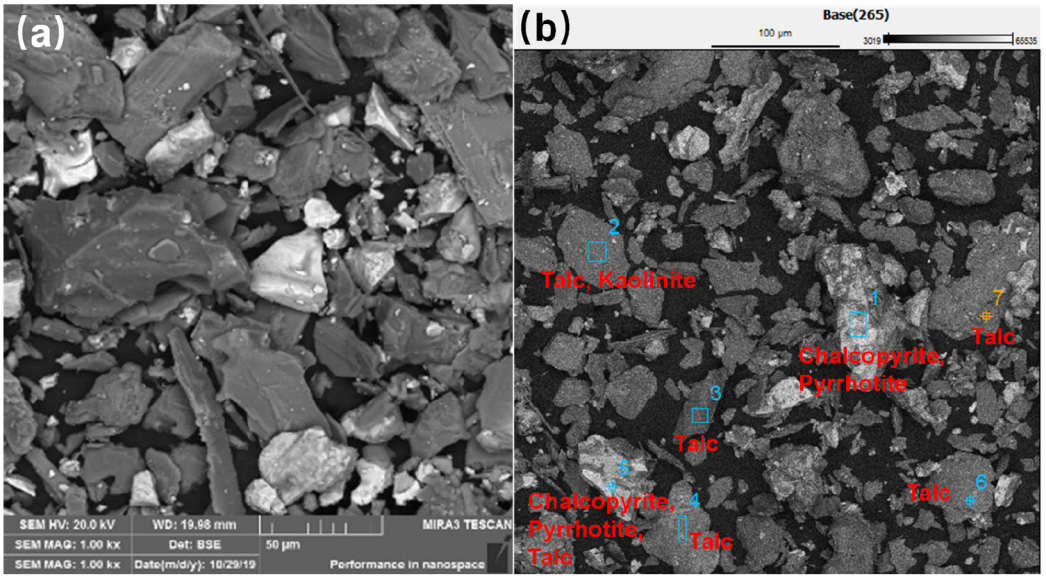


**Figure 2.** (a) Backscattered electron (BSE) micrograph of the raw concentrate sample; (b) points for EDS analyses and the phases identified by the EDS results.

of O, Mg, Al, Si, and Ca show a close correlation (Figure 3b, 3c, 3d, 3e, and 3g), which reflects the talc and kaolinite phases previously identified (Figure S1), while the Ca detected indicates the presence of unspecified Ca-Si-O phases within the concentrate matrix. Additionally, the Fe, Cu, and S distributions overlap due to the chalcopyrite and pyrrhotite present (Figure 3, Figure S1). In contrast, Ni was found to have a dispersed distribution that showed some correlation with Si. This finding suggests the possible existence of a $Ni_2SiO_3$ phase associated with talc, whereas the denser Ni-containing areas (indicated by a circle, Figure 3j) coexist with S as an NiS phase associated with chalcopyrite and pyrrhotite. Conversely, Ag was found to be distributed homogeneously across the analysis area, as silver is locked within the other phases present (Figure 3k). Nevertheless, quantitative EDS analysis determined a notably higher Ag content of 0.12% compared to total leaching (Figure S1), indicating that the overall distribution of Ag within the concentrate may be inhomogeneous.

**3.3. Baking of the Concentrate.** The XRD results displayed in Figure 4a show that with 200 °C, 3 h, and $H_2SO_4$ excess dosage of 20% of baking, the phases of kaolinite and pyrrhotite disappeared and that of chalcopyrite was weakened in the pattern, which indicates that the kaolinite and pyrrhotite were completely and chalcopyrite was partially decomposed.

As the temperature was increased to 250 °C under the same conditions, a new ferrous sulfate phase formed due to complete pyrrhotite and partial chalcopyrite oxidation, which also makes any mineral associated Ni accessible for leaching. Additionally, the intensity related to talc decreased with higher baking temperatures, highlighting the $SiO_2$ phase transformation from acid-soluble to the insoluble form. Thus, an optimal baking temperature of 250 °C and baking time of 4 h were selected (Figure 4b). With an analysis by the software *HighScrore*, the phase quantification of the baking process was determined. With 250 °C baking for 3 h, all the pyrrhotite and kaolinite transformed into ferrous sulfate and aluminum sulfate, respectively, and 2.1% of the talc transformed into caminite, and 1.2% of chalcopyrite was oxidized into copper sulfide and ferrous sulfate. Further, with the increase of baking time from 3 to 4 h, the oxidation of chalcopyrite continues to occur and 2.5% of chalcopyrite has transformed.

Pyrrhotite was found to disappear, and ferrous sulfate formed at an excess dosage of 0%, whereas with an excess dosage of 10%, the chalcopyrite XRD peaks became weaker/disappear, indicating this level was sufficient for chalcopyrite oxidation (Figure 4c). Additional weak peaks were formed during baking at an excess dosage of 10%, related to caminite ($Mg(SO_4)_2(OH)_2$) (Figure 4d); however, these were absent at higher excess dosage (20%). Similar behavior was observed when the excess dosage was increased from 0 to 5%, where peaks due to orschallite ($Ca_3(SO_3)_2SO_4{\cdot}12H_2O$) formation appeared and were then subsequently absent when the excess dosage was above 10%. Consequently, it can be speculated that during baking, talc transforms into caminite at an excess dosage of 10% before decomposition at higher excess dosage (20%) (eq 5), while Ca-Si-O phases become orschallite at an excess dosage below 5% prior to degradation at higher excess dosage (eq 6). Therefore, to ensure successful conversion of silicate-bearing materials to sulfate and acid insoluble $SiO_2$, an excess dosage of 10% was selected for baking. From the analysis, the following dominating and possible phase transformation paths are suggested (Table 4).

$$Mg_3Si_4O_{10}(OH)_2 + H_2SO_4(\text{concentrated}) \rightarrow Mg_3(SO_4)_2(OH)_2 + SiO_2 \quad (5)$$

$$\text{Ca-Si-O} + H_2SO_4(\text{concentrated}) \rightarrow Ca_3(SO_3)_2SO_4{\cdot}12H_2O + SiO_2 \quad (6)$$

When the excess dosage was 10%, 5.2% of the talc transformed into caminite, indicating that 87% of the total talc decomposed and, similarly, all the pyrrhotite and kaolinite transformed into ferrous sulfate and aluminum sulfate. The transformation of chalcopyrite was slight compared to phase quantification for Figure 4a and 4b, and the transformation quantity was only 2.6%, which is 74% of the total chalcopyrite in the raw concentrate.



https://doi.org/10.1021/acsomega.4c01560
ACS Omega 2024, 9, 26121−26132

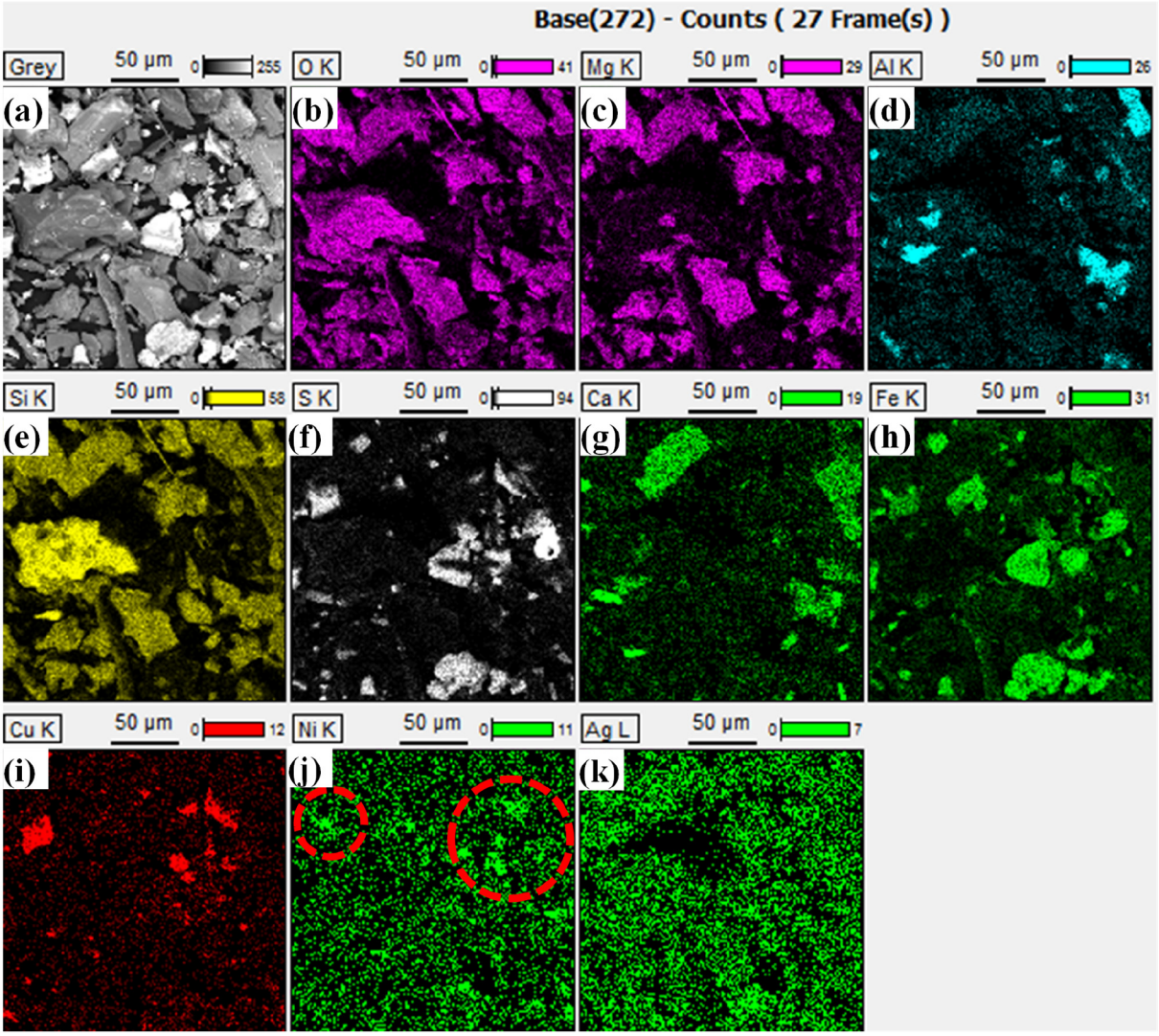


**Figure 3.** EDS mapping analysis of raw concentrate sample. (a) BSE image of the sample; (b) O, (c) Mg, (d) Al, (e) Si, (f) S, (g) Ca, (h) Fe, (i) Cu, (j) Ni, and (K) Ag map distribution.

Following these initial experiments, batch baking was investigated under optimized conditions (250 °C, 4 h, and excess dosage of 10%). The standard Gibbs free energy ($\Delta G^{\theta}$) of the dominated baked reactions at the optimized temperature of 250 °C were calculated with HSC-sim software, Table 5. It can be seen that the $\Delta G^{\theta}$ values at 250 °C of all reactions are negative values, indicating the thermodynamic feasibility for these reactions under the optimized conditions.

After baking was complete, the mineral phases of talc, chalcopyrite, pyrrhotite, kaolinite, and ferrous sulfate were all found to be dominating, while a concentrate color change from black to white gray was also observed (Figure S2). Furthermore, the particles of baked concentrate were found to be easy to grind and there was no associated hardening phenomenon evident. The composition of the baked concentrate was determined and is shown in Table 6. When compared to the chemical composition of raw concentrate, the main elemental contents in the baked concentrate are apparently decreased due to the oxidation of $S^{2-}$ into $SO_4^{2-}$.

**3.4. Development of the Leaching Process.** *3.4.1. Influence of Baking Process.* The leaching results show that the highest Ni extraction is gained in test T4 followed by tests T2 and T3 and finally test T1 (Figure 5a). The results indicate that both the baking process and the addition of $Cl^-$ can facilitate Ni leaching, although the effect of $Cl^-$ is more pronounced. The extraction of Ni from test T4 with the use of baking and addition of 20 g/L $Cl^-$ reaches 96% after 180 min, whereas in test T2 the extraction is only 75% in the absence of $Cl^-$. This suggests that pyrrhotite transformation during baking allowed the associated Ni to be liberated and $Cl^-$ promoted the leaching of Ni. In contrast, Cu extraction in tests T2 and T4 is very similar, at around 60% (Figure 5b). This suggests that copper exists in a different phase compared to Ni, and consequently the transformation due to baking could not liberate Cu in a similar manner as Ni.

The final Si extractions determined from the leaching experiments (test T1 and T3) with raw concentrate were 2% (with Fe(III)) and 5% (with Fe(III) and $Cl^-$), corresponding to the concentrations of 176 mg/L and 291 mg/L, Figure 6. Similar tests (T2 and T4) with the baked raw concentrate were found to have Si extraction levels <0.1% with dissolved concentrations of 23 mg/L and 10 mg/L. These results clearly demonstrate the impact of the baking process through transformation of Si to an acid-insoluble form.



https://doi.org/10.1021/acsomega.4c01560
ACS Omega 2024, 9, 26121−26132

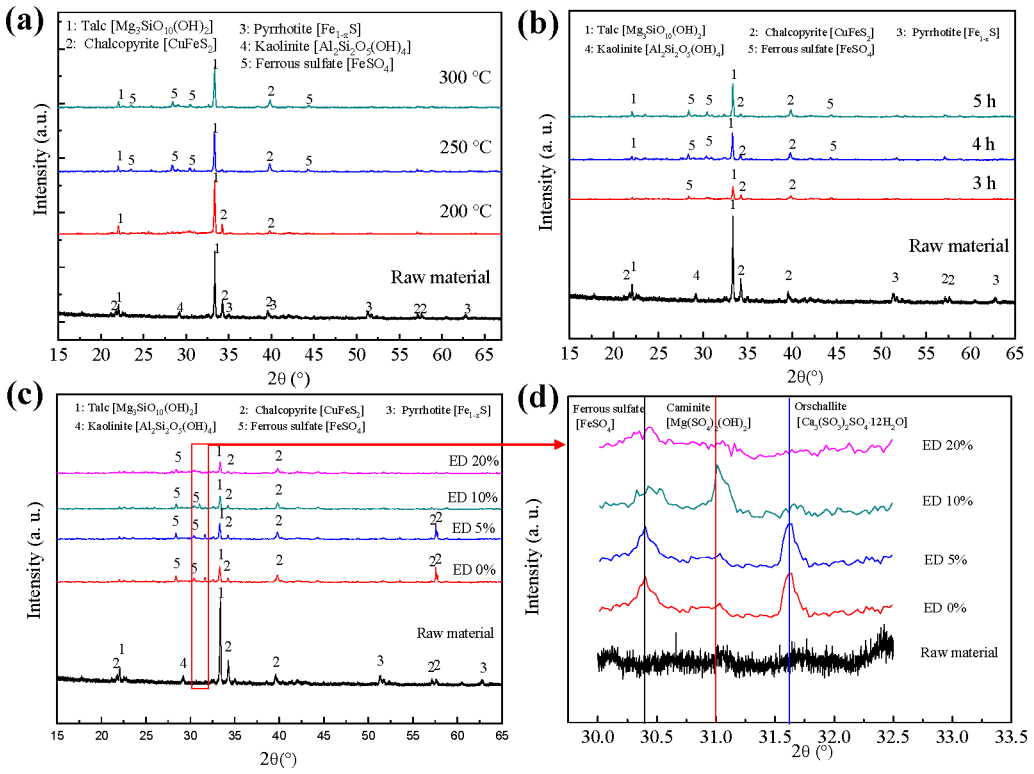


**Figure 4.** Comparison of the XRD patterns of the raw concentrate and baked concentrate in the case of (a) temperature of 200 °C, 250 °C, of 300 °C with excess dosage of 20% and time of 3 h; (b) time of 3, 4, and 5 h with temperature of 250 °C and excess dosage of 5%; (c) ED of 0%, 5%, 10%, and 20% with time of 4 h and 250 °C. (d) XRD patterns between 30.0° to 32.5° from figure (c).

**Table 4. Baking Process Phase Transformation Pathways**

| | | | Notes of conditions | | |
|---|---|---|---|---|---|
| | Initial phase | Baked phase | *T* (°C) | *t* (h) | ED (%) |
| Dominating phase transformation | Pyrrhotite | Ferrous sulfate | 250, 300 | 3, 4, 5 | 0−20 |
| | Talc | Caminite | 250 | 4 | 10 |
| | Chalcopyrite | Ferrous sulfate, Cu-phase | 200, 250, 300 | 3, 4, 5 | 0−20 |
| Possible phase transformation | Kaolinite | Aluminum sulfate | 250, 300 | 3, 4, 5 | 0−20 |
| | Ca-Si-O phase | Orschallite | 250 | 4 | 0, 5 |

**Table 5. Standard Gibbs Free Energy of the Dominated Baking Reactions at 250 °C**

| Reaction | $\Delta G^{\theta}$(523 K) (kJ/mol) |
|---|---|
| $FeS_{(s)} + 2O_{2(g)} \rightarrow FeSO_{4(s)}$ | −153.2 |
| $2CuFeS_{2(s)} + 5O_{2(g)} \rightarrow Cu_2S_{(s)} + 2FeSO_{4(s)} + SO_{2(g)}$ | −358.3 |
| $Mg_3Si_4O_{10}(OH)_2 + 2H_2SO_4$(concentrated) → $Mg_3(SO_4)_2(OH)_2 + 4SiO_2 + 2H_2O$ | −37.3 |
| $Al_2Si_2O_5(OH)_4 + 3H_2SO_4$(concentrated) → $Al_2SO_4 + 2SiO_2 + 5H_2O$ | −59.3 |

**Table 6. Elemental Composition of the Baked Concentrate under the Optimized Conditions[a]**

| BEs | Fe | Si | Mg | Cu | Al | Ni | Ca |
|---|---|---|---|---|---|---|---|
| wt % | 18.8 | 10.9 | 5.80 | 2.30 | 1.50 | 1.00 | 0.90 |
| **PMs** | **Pd** | **Ag** | **Pt** | **Au** | | | |
| g/t | 14.93 | 17.12 | 2.10 | 1.07 | | | |

[a]250 °C, 4 h, and excess dosage of 10%.

*3.4.2. Influence of Cl⁻ and Fe(III).* Prolonging leaching time to 300 min and increasing Fe(III) concentration to 10.0 g/L (test T5) were also investigated, expecting higher extractions. However, in test T5, Ni extraction was only 68% at 300 min and Cu 64%. On the other hand, for test T6 with 10 g/L Fe(III) and 20 g/L $Cl^-$, the Ni extraction was as high as 97% whereas Cu remained at 60%. The extension of the leaching time and increase of the Fe(III) concentration could not increase Ni and Cu in either test T5 or T6 (Figure 7a and 7b).

Conversely, in the absence of $Cl^-$, the kinetics of Ni leaching is poor and significantly lower extractions of only ca. 60% were obtained after 180 min (Figure 7(a). It was also observed that in the absence of Fe(III) addition, but with 20 g/L $Cl^-$ (test T7; Figure 7c), the Cu extraction was low, decreasing from 30% to 3% after 20 min. This behavior is probably attributed to the formation of antlerite ($CuSO_4{\cdot}2Cu(OH)_2$)[21] or secondary covellite (CuS),[39] which has been previously reported to occur in the presence of sufficient sulfate or chloride. For solving this problem, we suggest a two-stage leaching for the recovery of Cu from the leach residue bearing antlerite or secondary covellite by using a low concentration of ferric chloride solution as lixiviant.

These show the critical role of $Cl^-$ and Fe(III) for the leaching of Ni and Cu from the baked concentrate.



https://doi.org/10.1021/acsomega.4c01560
ACS Omega 2024, 9, 26121−26132

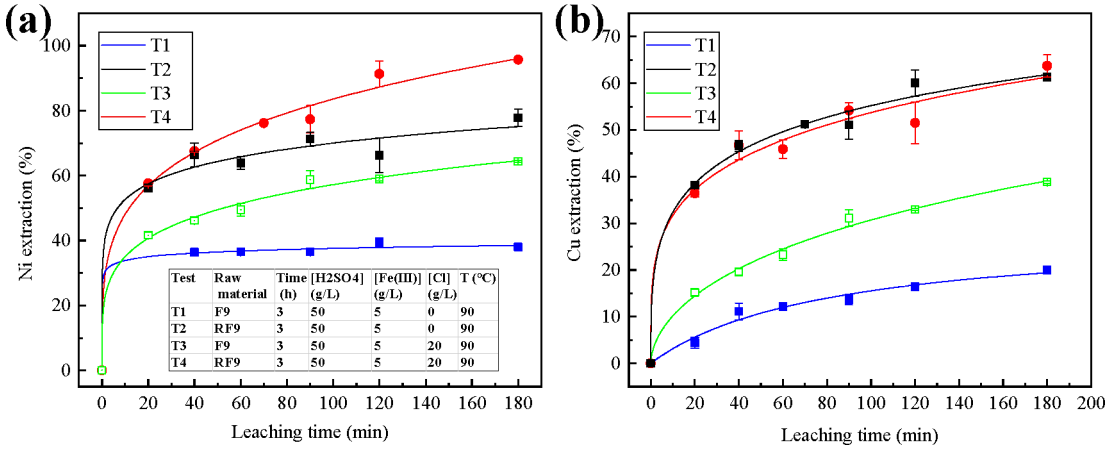


| Test | Raw material | Time (h) | [H2SO4] (g/L) | [Fe(III)] (g/L) | [Cl] (g/L) | T (°C) |
|---|---|---|---|---|---|---|
| T1 | F9 | 3 | 50 | 5 | 0 | 90 |
| T2 | RF9 | 3 | 50 | 5 | 0 | 90 |
| T3 | F9 | 3 | 50 | 5 | 20 | 90 |
| T4 | RF9 | 3 | 50 | 5 | 20 | 90 |

**Figure 5.** Comparison of extraction of (a) Ni and (b) Cu from tests T1−T4.

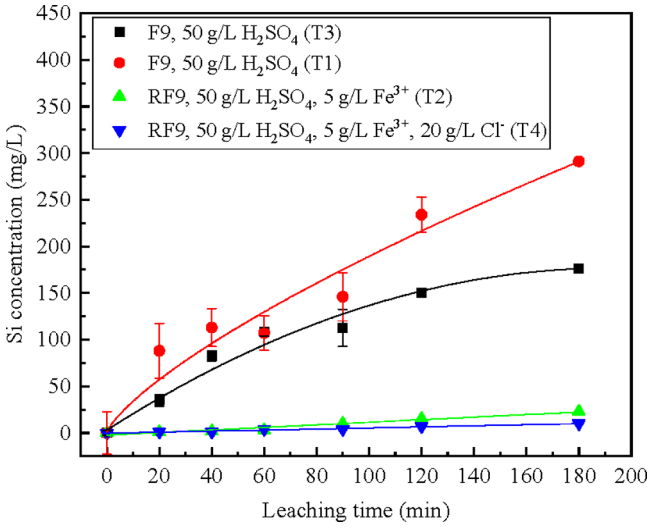


**Figure 6.** Comparison of the leaching concentration of Si from the tests using raw concentrate F9 (tests T1 and T3) and baked concentrate RF9 (tests T2 and T4) as raw materials.

*3.4.3. Role of $Cl^-$ and Fe(III).* It has been reported that the activation energy of the dissolution reaction of chalcopyrite in ferric chloride (eq 7) is lower than that in ferric sulfate media (eq 8),[40] and the dissolution rate of pyrrhotite relies on the $Cl^-$ significantly due to a very low activation energy for the dissolution reaction in chloride media (7 kcal/mol).[41] Moreover, it has been proven that the dissolution rate of pyrrhotite in nonoxidative conditions (typically $Cl^-$, eq 9) is 3 orders of magnitude higher than in oxidative conditions (typically $Fe^{3+}$ (eq 10)).[42,43]

$$CuFeS_{2(s)} + 4FeCl_3 \rightarrow CuCl_2 + 5FeCl_2 + 2S_{(s)}$$
$$\Delta G^{\theta}_{1} = -59.9\ \text{kJ/mol} \quad (7)$$

$$CuFeS_{2(s)} + 2Fe_2(SO_4)_3 \rightarrow CuSO_4 + 5FeSO_4 + 2S_{(s)}$$
$$\Delta G^{\theta}_{2} = -81.0\ \text{kJ/mol} \quad (8)$$

$$FeS_{(s)} + 2FeCl_3 \rightarrow 3FeCl_2 + S_{(s)}$$
$$\Delta G^{\theta}_{3} = -126.9\ \text{kJ/mol} \quad (9)$$

$$FeS_{(s)} + Fe_2(SO_4)_3 \rightarrow 3FeSO_4 + S_{(s)}$$
$$\Delta G^{\theta}_{4} = -126.8\ \text{kJ/mol} \quad (10)$$

For the oxidative dissolution of pyrrhotite in the acidic ferric sulfate-chloride media, the redox between 450 and 600 mV was not affected by the addition of $Cl^-$, and thus, there was no essential change for the oxidation of $S^{2-}$. However, for the nonoxidative dissolution in acidic sulfate-chloride media in the absence of ferric ions, $Fe^{2+}$ releases from the surface of pyrrhotite and coordinates with $Cl^-$ to form $FeCl^-$ and $FeCl_2$ species, and after a critical accumulation of charge, negative charge is released from the surface as $HS^-$.[44] Therefore, when $Cl^-$ was added into ferric sulfate media, oxidative dissolution of pyrrhotite did not change essentially, whereas nonoxidative dissolution occurred, resulting in a significant increase of dissolution rate and thereby liberation of the associated Ni. In addition, the leaching of Cu was originally facilitated by $Cl^-$; however, the possible precipitation of secondary covellite (eq 11) or antlerite (eq 12) could counteract that effect, resulting in similar Cu extraction in the presence and absence of $Cl^-$.

$$CuFeS_2 + [CuCl]^+ \rightarrow 2CuS + Fe^{2+} + Cl^-$$
$$\Delta G^{\theta}_{5} = -31.26\ \text{kJ/mol} \quad (11)$$

$$3CuSO_4 + 4H_2O \rightarrow CuSO_4 \cdot 2Cu(OH)_2 + 2H_2SO_4$$
$$\Delta G^{\theta}_{6} = -2142.5\ \text{kJ/mol} \quad (12)$$

*3.4.4. Comprehensive Effect of Variables.* The effects of variables including concentration of Fe(III), $Cl^-$, and $H_2SO_4$ and temperature on Ni and Cu extraction are summarized in Figure 8. Significant plateaus appeared in Figure 8a−c, indicating the optimized parameters of 5g/L Fe(III), 20g/L $Cl^-$, and 50g/L $H_2SO_4$ for Ni and Cu extraction. Moreover, the increased temperature enhanced the extraction of Ni and Cu significantly (Figure 8d), and 90 °C was therefore selected as the optimal temperature.

**3.5. Leach Residue and Enrichment of the PMs.** Leach residue ($R_{T4}$) from the experiment with baked raw material in the presence of Fe(III) and $Cl^-$ (test T4) was characterized by SEM-EDS mapping analysis. The existence of a sulfur phase formed through the oxidation of $S^{2-}$ and the chalcopyrite and NiS phase was detected in the residue (Figure 9). From the initial analysis of the raw concentrate, the presence of a NiS phase could not be readily determined. Nevertheless, the Ni


https://doi.org/10.1021/acsomega.4c01560
ACS Omega 2024, 9, 26121−26132

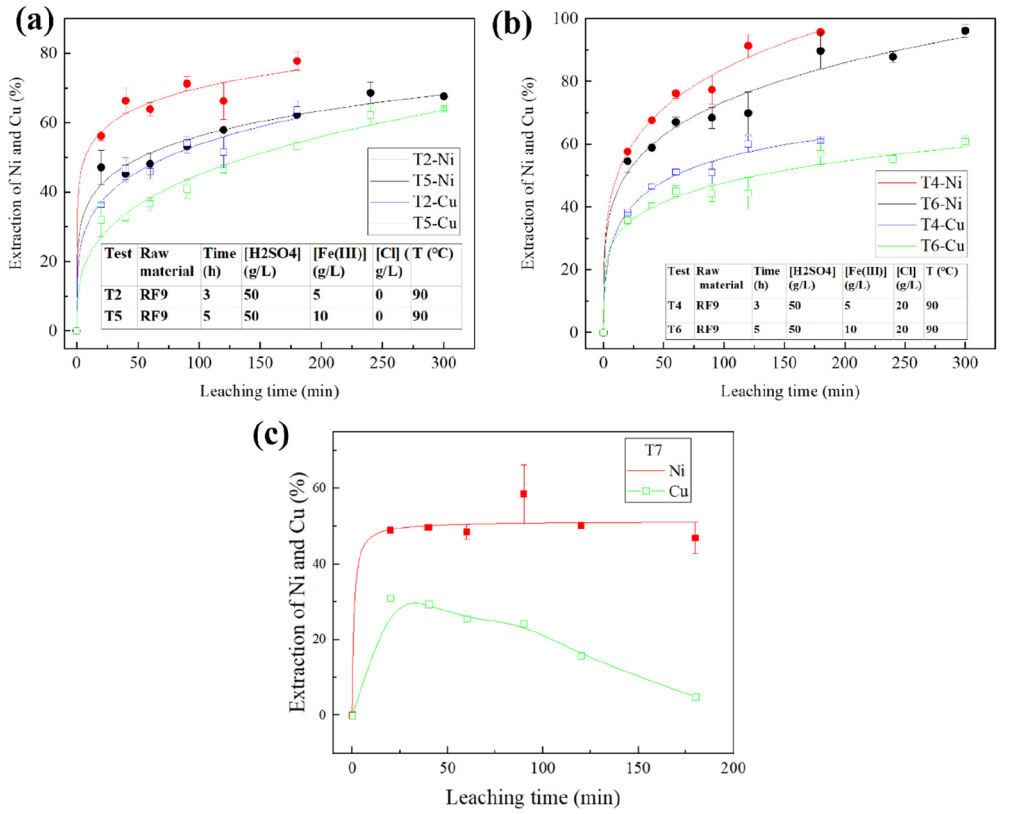


**Figure 7.** Comparison of extraction of Ni and Cu from (a) tests T2 and T5, (b) tests T4 and T6, and (c) test T7 (0 g/L Fe(III) and 20 g/L $Cl^-$).

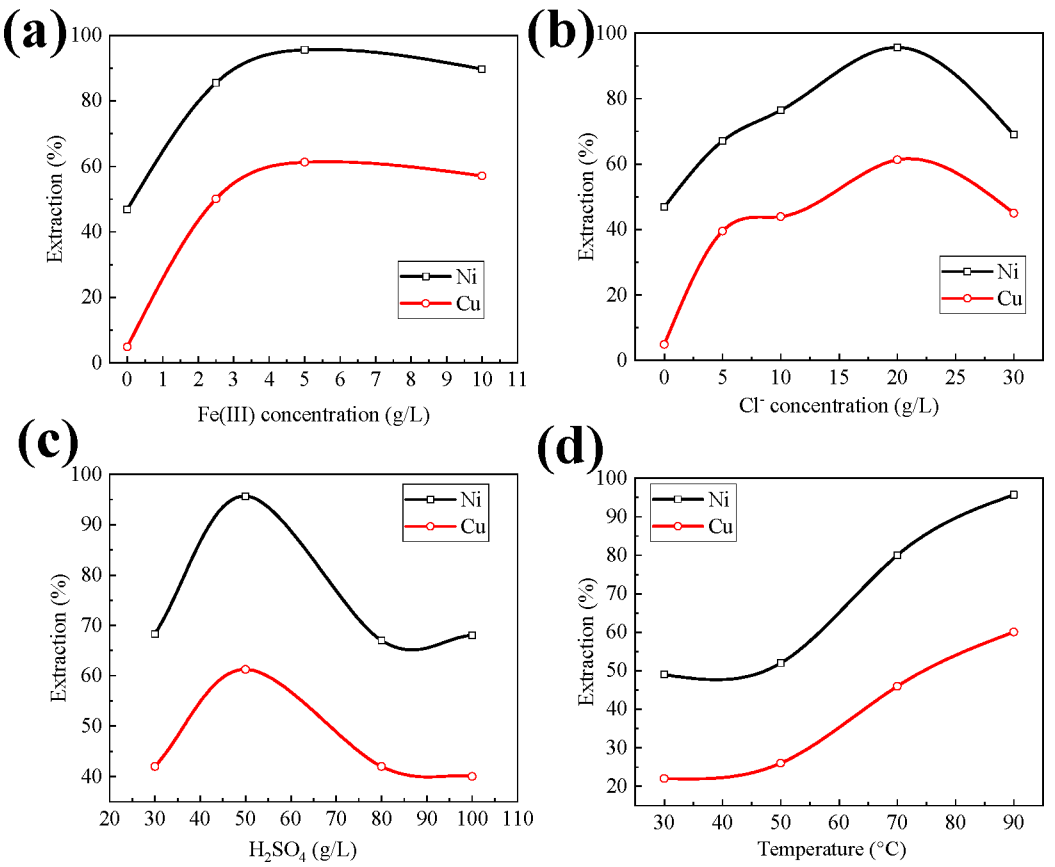


**Figure 8.** Effect of the concentration of (a) Fe(III), (b) $Cl^-$, and (c) $H_2SO_4$ and (d) temperature on the extraction of Ni and Cu.



https://doi.org/10.1021/acsomega.4c01560
ACS Omega 2024, 9, 26121−26132

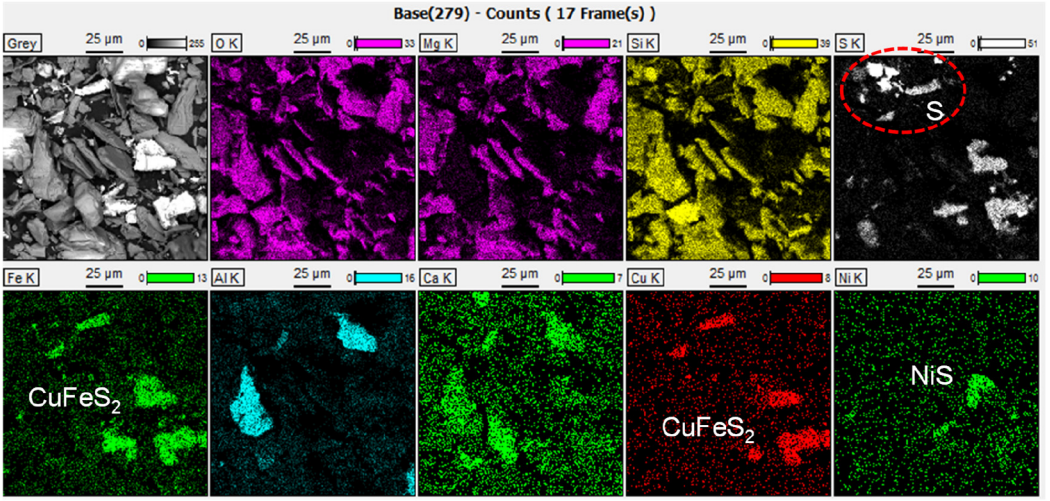


**Figure 9.** Elemental distribution of the leach residue obtained from test T4 (T4, RF9, 90 °C, 50 g/L $H_2SO_4$, 5.0 g/L Fe(III), 20.0 g/L $Cl^-$).

that is closely associated with pyrrhotite is able to be dissolved during the leaching process, as the pyrrhotite is transformed to $FeSO_4$ by the baking process. Consequently, any remaining undissolved Ni-S phase detected in the resultant residue is characteristic of the original Ni phase present in the concentrate.

Comparison of the PMs/PGMs contents of the leach residue is displayed in Table 7 and clearly highlights that Pd, Au, and Pt are enriched into the leach residue. Pd shows the highest level of enrichment, as its content doubled from that in the AHM concentrate. After test T4, although Pd extraction was only 0.79% with concentration of 4.6 μg/L, Ag was as high as 89.4% with a concentration of 598 μg/L. With a metallurgical balance analysis, the percentage of PMs in the leach residue plus the amount in the PLS was in the range of 97.5−103%, indicating an acceptable balance for the leaching process. As can be seen, the residue ($R_{T4}$) is rich in Pd, Au, and Pt, which is directly suitable for further PMs recovery.

**Table 7. PM/PGMs Contents of Raw Concentrate, Baked Concentrate under Optimized Conditions,[a] and Leach Residue from Test T4[b] and Related Leaching Concentration and Extractions from Test T4**

| Sample | Pd | Ag | Au | Pt |
|---|---|---|---|---|
| Raw concentrate (g/t) | 14.9 | 17.1 | 1.07 | 2.10 |
| Baked concentrate (g/t) | 11.7 | 13.4 | 0.84 | 1.64 |
| Leach residue (g/t) | 30.3 | 12.8 | 3.07 | 3.79 |
| PLS from test T4 (μg/L) | 4.63 | 598 | 12.1 | <0.20 |
| Leaching efficiency of PMs from test T4 (%) | 0.79 | 89.4 | 29.0 | 0 |
| Leach residue (%) + PLS (%) | 98.7 | 103 | 99.2 | 97.5 |

[a]250 °C, 4 h, and excess dosage of 10%. [b]Baked concentrate, 3 h, 50 g/L $H_2SO_4$, 5 g/L Fe(III), 20 g/L $Cl^-$, 90 °C.

**3.6. Reagents and Energy Consumption.** The consumption of leaching reagents was estimated by simulating the baking and leaching processes using HSC-Sim software. Results for the tested conditions are presented in Table S2 and were normalized for 1 kg of extracted Ni after 180 min of leaching. The acid consumption in the leaching reactions was minimal due to the elemental sulfur oxidation; therefore, acid consumption was assumed to mainly be related to adjustment of the leaching chemistry, associated reactions and evaporation that occur during the baking process. During baking, the acid loading was 580 kg/$t_{concentrate}$ under the ideal conditions (10% excess dosage) and 800−2650 kg/$t_{concentrate}$ in leaching between the different test conditions. The values for $Fe_2(SO_4)_3$ and NaCl were determined to be between 240−980 and 220−1340 kg/$t_{concentrate}$, respectively.

As can be seen in Figure 10, acid consumption in the baking step is comparably low when its positive effect on Ni recovery is considered. Normalization of the results for Ni shows that for the baseline leaching conditions—50 g/L $H_2SO_4$, 20 g/L $Cl^-$, and 5 g/L Fe(III)— the optimal reagents consumption and omission of the baking step have little effect on the values of acid consumption. The high overall reagent consumption in leaching could be decreased by increasing the S/L ratio and circulating the leaching solution in the process. Further

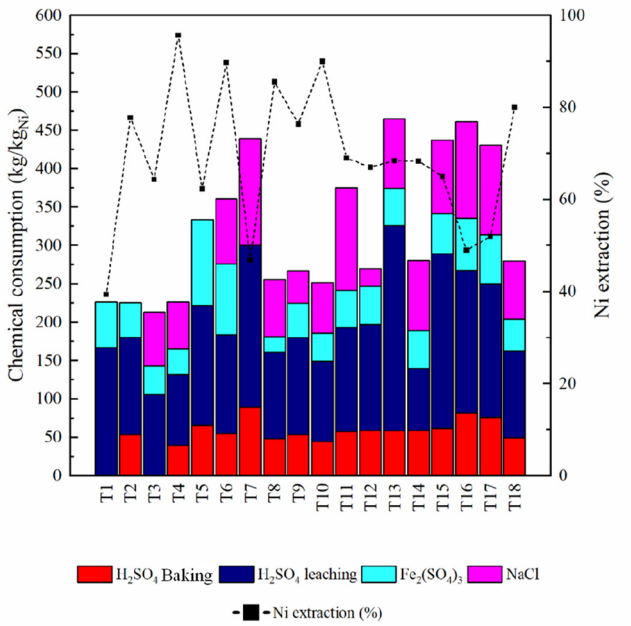


**Figure 10.** Leaching reagent consumption under the experimental conditions for 1 kg of extracted nickel. Ni extraction after 180 min (%) is shown for clarity.



https://doi.org/10.1021/acsomega.4c01560
ACS Omega 2024, 9, 26121−26132

information about chemical and energy consumption can be found in the Supporting Information.

## 4. CONCLUSIONS

Characterization, baking, and leaching for the Suhanko Ahmavaara concentrate were investigated, and subsequent predication modeling was also carried out.

(1) The Suhanko Ahmavaara concentrate contained mineral phases of talc, chalcopyrite, pyrrhotite, and kaolinite, the main base elements Ni, Cu, Fe, Mg, Al, Ca, and Si, and the PMs Pd, Pt, Au, and Ag; Ni existed as NiS that associated with pyrrhotite.

(2) The optimal baking conditions of 250 °C, 4 h, and ED of 10% were experimentally obtained; during the baking pyrrhotite and chalcopyrite oxidized into ferrous sulfate and unidentified Cu-phase, leading the liberation of Ni.

(3) Leaching tests for the baked and unbaked concentrate in the Fe(III)-$Cl^-$-$H_2SO_4$ system were conducted. It was found that the baking process facilitated the leaching of Ni and controlled the leaching of Si significantly via the conversion of acid-soluble silicate into the insoluble form. $Cl^-$ and Fe(III) were critical for the high extraction of Ni and Cu in leaching, of which Fe(III) as oxidant oxidized $S^{2-}$ into S, and $Cl^-$ increased the dissolution rate of pyrrhotite and chalcopyrite significantly due to the low activation energy of the nonoxidative reaction. However, Cu during the leaching precipitated as possible phase copper sulfide or antlerite, consequently inhibiting the Cu recovery. Furthermore, the optimal parameters (50 g/L $H_2SO_4$, 5 g/L Fe(III), 20 g/L $Cl^-$, and 90 °C) of the leaching test were obtained. Under these conditions, the extraction of Ni, Cu, and Ag reached 97%, 60%, and 89% respectively, whereas Si extraction was below 0.1%. Concurrently, PMs (Pd, Pt, and Au) were enriched to 30.3 g/t, 3.8 g/t, and 3.1 g/t in the leaching residue.

(4) The baking process is beneficial in decreasing the consumption of reagents when weighed against Ni extraction. The leaching reagents are not consumed during leaching reactions, and further reagent recirculation could substantially reduce operating costs and the associated environmental impacts.

## ■ ASSOCIATED CONTENT

### Supporting Information

The Supporting Information is available free of charge at https://pubs.acs.org/doi/10.1021/acsomega.4c01560.

Two figures and three tables including additional information regarding the EDS results of the point scan for the raw material, the EDS spectrum, photographs of the F9 sample before and after baking, chemical and energy consumptions, and references. (PDF)

## ■ AUTHOR INFORMATION


### Corresponding Authors

**Pingchao Ke** − *The State Key Laboratory of Nuclear Resources and Environment and School of Water Resources and Environmental Engineering, East China University of Technology, Nanchang 330000, China; Hydrometallurgy and Corrosion, Department of Chemical and Metallurgical Engineering (CMET), School of Chemical Engineering, Aalto University, FI-00076 Aalto, Finland;* orcid.org/0000-0003-4679-1162; Email: kepingchao@ecut.edu.cn

**Mari Lundström** − *Hydrometallurgy and Corrosion, Department of Chemical and Metallurgical Engineering (CMET), School of Chemical Engineering, Aalto University, FI-00076 Aalto, Finland*; Email: mari.lundstrom@aalto.fi

### Authors

**Marja Rinne** − *Hydrometallurgy and Corrosion, Department of Chemical and Metallurgical Engineering (CMET), School of Chemical Engineering, Aalto University, FI-00076 Aalto, Finland;* orcid.org/0000-0002-1223-0511

**Taina Kalliomäki** − *Hydrometallurgy and Corrosion, Department of Chemical and Metallurgical Engineering (CMET), School of Chemical Engineering, Aalto University, FI-00076 Aalto, Finland*

**Zulin Wang** − *Hydrometallurgy and Corrosion, Department of Chemical and Metallurgical Engineering (CMET), School of Chemical Engineering, Aalto University, FI-00076 Aalto, Finland;* orcid.org/0000-0002-2234-7983

**Pyry-Mikko Hannula** − *Hydrometallurgy and Corrosion, Department of Chemical and Metallurgical Engineering (CMET), School of Chemical Engineering, Aalto University, FI-00076 Aalto, Finland;* orcid.org/0000-0001-9844-2234

**Benjamin P. Wilson** − *Hydrometallurgy and Corrosion, Department of Chemical and Metallurgical Engineering (CMET), School of Chemical Engineering, Aalto University, FI-00076 Aalto, Finland;* orcid.org/0000-0002-2874-6475

Complete contact information is available at: https://pubs.acs.org/10.1021/acsomega.4c01560


### Author Contributions

The first author was working at Aalto University as a researcher, and currently, he is an assistant professor at East China University of Technology. Most of this work was completed at Aalto University.

### Notes

The authors declare no competing financial interest.

## ■ ACKNOWLEDGMENTS

The authors thank Ville Kivinen for drying and dividing the concentrate sample, Tao Jiang, Pengbo Zhou, and Zhihong Liu from Central South University, China, for their kind help on the baking experiments, and Petteri Halli and Fang Hu from Aalto University and Juha Rissanen and Dominic Claridge from Suhanko Arctic Platinum Company for providing the information on the concentrate and their helpful discussion. This project was supported by a BATCircle project (grant number 4853/31/2018), open funding from Guangdong Provincial Key Laboratory of Radioactive and Rare Resource Utilization (grant number 2018B030322009), a Jiangxi Province Youth Science Foundation Project (grant number 20202BABL21), and the Academy of Finland's RawMatTERS Finland Infrastructure (RAMI).

## ■ REFERENCES

(1) Brininstool, M. Copper Statistics and Information. USGS, https://minerals.usgs.gov/minerals/pubs/commodity/copper/mcs-2020-copper.pdf.

(2) Schnebele, E. K. Nickel Statistics and Information. USGS, https://minerals.usgs.gov/minerals/pubs/commodity/nickel/mcs-2020-nicke.pdf.
(3) Zeng, X.; Li, J.; Singh, N. Recycling of spent lithium-ion battery: A critical review. *Critical Reviews in Environmental Science and Technology*. **2014**, *44* (10), 1129−1165.
(4) Yu, H.; Yang, H.; Chen, K.; Yang, L.; Huang, M.; Wang, Z.; Lv, H.; Xu, C.; Chen, L.; Luo, X. Non−closed−loop recycling strategies for spent lithium−ion batteries: Current status and future prospects. *Energy Storage Materials* **2024**, *67*, No. 103288.
(5) Liu, T.; Li, F.; Jin, Z.; Yang, Y. Acidic leaching of potentially toxic metals cadmium, cobalt, chromium, copper, nickel, lead, and zinc from two Zn smelting slag materials incubated in an acidic soil. *Environ. Pollut.* **2018**, *238*, 359−368.
(6) Dutrizac, J. E. The leaching of sulphide minerals in chloride media. *Hydrometallurgy*. **1992**, *29*, 1−45.
(7) Harris, D. C. Silver-bearing chalcopyrite, a principal source of silver in the Izok Lake massive sulfide deposit: confirmation by electron and proton microprobe analyses. *Canadian Mineralogist* **1984**, *22* (3), 493−498.
(8) Mpinga, C. N.; Eksteen, J. J.; Aldrich, C.; Dyer, L. Atmospheric leach process of high-chromitite PGM-bearing oxidized mineralized ore through a single-stage and two-stage techniques. *Minerals Engineering* **2018**, *125* (15), 165−175.
(9) Syed, S. Recovery of gold from secondary sources—A review. *Hydrometallurgy* **2012**, *115*−*116*, 30−51.
(10) Dorfling, C.; Akdogan, G.; Bradshaw, S. M.; Eksteen, J. J. Determination of the relative leaching kinetics of Cu, Rh, Ru and Ir during the sulphuric acid pressure leaching of leach residue derived from Ni−Cu converter matte enriched in platinum group metals. *Minerals Engineering* **2011**, *24* (6), 583−589.
(11) Lung, T. N. The history of copper cementation on iron — The world's first hydrometallurgical process from medieval China. *Hydrometallurgy* **1986**, *17*, 113−129.
(12) Oluokun, O. O.; Otunniyi, I. O. Kinetic analysis of Cu and Zn dissolution from printed circuit board physical processing dust under oxidative ammonia leaching. *Hydrometallurgy*. **2020**, *193*, No. 105320.
(13) Kruesi, P. R.; Goens, D. N. Process for the recovery of copper from its sulfide ores. U.S. Patent US3901776A, 1975.
(14) Paynter, J. C. A review of copper hydrometallurgy. *Journal of the South African. Institute of Mining. and Metallurgy* **1974**, *74* (4), 158−170.
(15) McDonald, R. G.; Muir, D. M. Pressure oxidation leaching of chalcopyrite. Part I. Comparison of high and low temperature reaction kinetics and products. *Hydrometallurgy* **2007**, *86*, 191−205.
(16) Palmer, C. M.; Johnson, G. D. The Activox® process: growing significance in the nickel industry. *JOM: The Journal of the Minerals, Metals and Materials Society* **2005**, *57* (7), 40−47.
(17) Hyvärinen, O.; Hämäläinen, M. HydroCopper—a new technology producing copper directly from concentrate. *Hydrometallurgy*. **2005**, *77*, 61−65.
(18) Lu, J.; Dreisinger, D. Copper leaching from chalcopyrite concentrate in Cu(II)/Fe(III) chloride system. *Minerals Engineering* **2013**, *45*, 185−190.
(19) Zhang, R.; Mao, Y.; Liu, C.; Ni, W. Synergistic catalytic effect of chloride ion and ammonium ion on the leaching of chalcopyrite in sulfuric acid solution. *Minerals Engineering* **2022**, *185*, No. 107686.
(20) Ma, Y.; Yang, Y.; Fan, R.; Gao, X.; Zheng, L.; Chen, M. Chalcopyrite leaching in ammonium chloride solutions under ambient conditions: Insight into the dissolution mechanism by XANES, Raman spectroscopy and electrochemical studies. *Minerals Engineering* **2021**, *170*, No. 107063.
(21) Balaz, P.; Boldizarova, E.; Achimovicova, M.; Kammel, R. Leaching and dissolution of a pentlandite concentrate pretreated by mechanical activation. *Hydrometallurgy* **2000**, *57*, 85−96.
(22) Li, P.; Shimaoka, T. Recovery of Zn and Cu from municipal solid waste incineration fly ash by integrating ammonium leaching and ammonia removal. *Waste Management* **2024**, *178*, 115−125.
(23) Senanayake, G. Chloride assisted leaching of chalcocite by oxygenated sulphuric acid via Cu(II)−OH−Cl. *Minerals Engineering* **2007**, *20* (11), 1075−1088.
(24) Karppinen, A.; Seisko, S.; Lundström, M. Atmospheric leaching of Ni, Co, Cu, and Zn from sulfide tailings using various oxidants. *Minerals Engineering* **2024**, *207*, No. 108576.
(25) Arpalahti, A.; Lundström, M. The leaching behavior of minerals from a pyrrhotite-rich pentlandite ore during heap leaching. *Minerals Engineering* **2018**, *119*, 116−125.
(26) Intec Ltd Superior and Sustainable Metals Production. The Intec Copper Process. Sydney, Intec Ltd, 2008; 1−20.
(27) Fleming, C. A. Platsol$^{TM}$ process provides a viable alternative to smelting. SGS Minerals Services., 2002; Technical Paper 2002-01.
(28) Hu, F.; Hu, H.; Yang, J.; Luo, Y.; Lundström, M.; Ji, G.; Hu, J. Preferential extraction of Ni(II) over Co(II) by arylsulphonic acid in the presence of pyridinecarboxylate ester: Experimental and DFT calculations. *J. Mol. Liq.* **2019**, *291*, No. 111253.
(29) Sinisalo, P.; Lundström, M. Refining Approaches in the Platinum Group Metal Processing Value Chain-A Review. *Metals* **2018**, *8*, 203.
(30) Fan, Y.; Liu, Y.; Niu, L.; Zhang, W.; Zhang, T. Leaching of silver from silver-bearing residue by a choline chloride aqueous solution and the sustained deposition of silver on copper. *Hydrometallurgy* **2020**, *197*, No. 105454.
(31) Karppinen, A.; Seisko, S.; Nevatalo, L.; Wilson, B. P.; Yliniemi, K.; Lundström, M. Gold recovery from cyanidation residue by chloride leaching and carbon adsorption − Preliminary results from CICL process. *Hydrometallurgy* **2024**, *226*, No. 106304.
(32) Koohestani, B.; Darban, A. K.; Mokhtari, P.; Darezereshki, E.; Yilmaz, E.; Yilmaz, E. Influence of hydrofluoric acid leaching and roasting on mineralogical phase transformation of pyrite in sulfidic mine tailings. *Minerals* **2020**, *10* (6), 513.
(33) Hapid, A.; Zullaikah, S.; Mahfud; Kawigraha, A.; Sudiyanto, Y.; Benita Nareswari, R.; Quitain, A. T. Oxidation of sulfide mineral and metal extraction analysis in the microwave-assisted roasting pretreatment of refractory gold ore. *Arabian Journal of Chemistry* **2024**, *17* (1), No. 105447.
(34) Konadu, K. T.; Huddy, R. J.; Harrison, S. T. L.; Osseo-Asare, K.; Sasaki, K. Sequential pretreatment of double refractory gold ore (drgo) with a thermophilic iron oxidizing archeaon and fungal crude enzymes. *Minerals Engineering* **2019**, *138*, 86−94.
(35) Yang, T.; Dai, M.; Tang, G.; Guo, Z.; Yang, Y.; Jiao, H. Effect of an electro-assisted biochemical cycle reactor on bio-oxidation of gold ore. *Minerals Engineering* **2024**, *209*, No. 108630.
(36) Schindler, M.; Legrand, C. A.; Hochella, M. F. Alteration, adsorption and nucleation processes on clay-water interfaces: mechanisms for the retention of uranium by altered clay surfaces on the nanometer scale. *Geochim. Cosmochim. Acta* **2015**, *153*, 15−36.
(37) Zhang, Y.; Hua, Y.; Gao, X.; Xu, C.; Li, J.; Li, Y.; Zhang, Q.; Xiong, L.; Su, Z.; Wang, M. Recovery of zinc from a low-grade zinc oxide ore with high silicon by sulfuric acid curing and water leaching. *Hydrometallurgy* **2016**, *166*, 16−21.
(38) Wang, X.; Sun, Z.; Liu, Y.; Min, X.; Guo, Y.; Li, P.; Zheng, Z. Effect of particle size on uranium bioleaching in column reactors from a low-grade uranium ore. *Bioresour. Technol.* **2019**, *281*, 66−71.
(39) Lundström, M.; Liipo, P.; Taskinen, J.; Aromaa, J. Copper precipitation during leaching of various copper sulfide concentrates with cupric chloride in acidic solutions. *Hydrometallurgy* **2016**, *166*, 136−142.
(40) Nicol, M. J.; Akilan, C. The kinetics of the dissolution of chrysocolla in acid solutions. *Hydrometallurgy* **2018**, *178*, 7−11.
(41) Ingraham, T. R.; Parsons, H. W.; Cabri, L. J. Leaching of pyrrhotite with hydrochloric acid. *Canadian Metallurgical Quarterly* **1972**, *11* (2), 407−411.
(42) Thomas, J. E.; Skinner, W. M.; Smart, R. S. C. A mechanism to explain sudden changes in rates and products for pyrrhotite dissolution in acid solution. *Geochim. Cosmochim. Acta* **2001**, *65* (1), 1−12.


https://doi.org/10.1021/acsomega.4c01560
*ACS Omega* 2024, 9, 26121−26132

(43) Pratt, A. R.; Muir, I. J.; Nesbitt, H. W. X-ray photoelectron and Auger electron studies of pyrrhotite and mechanism of air oxidation. *Geochim. Cosmochim. Acta* **1994**, *58* (2), 827−841.
(44) Jones, C. F.; Le Count, S.; Smart, R. St. C.; White, T. J. Compositional and structural alteration of pyrrhotite surfaces in solution: XPS and XRD studies. *Appl. Surf. Sci.* **1992**, *55*, 65−85.



https://doi.org/10.1021/acsomega.4c01560
*ACS Omega* 2024, 9, 26121−26132